

Supporting information: Optimized colloidal growth of hexagonal close-packed Ag nanoparticles and their stability under catalytic conditions

Michaël Gebruers,^a Rafikul A. Saha,^a Alexey V. Kubarev,^a Lotte Clinckemalie,^b Yuhe Liao,^c Elke Debroye,^b Bo Weng^a and Maarten B. J. Roeflaers*^a

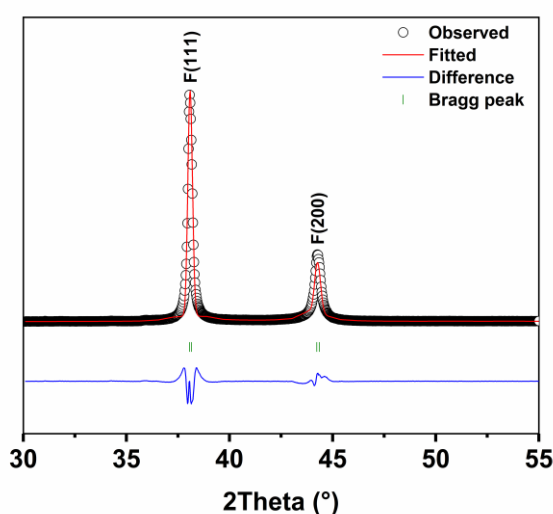
^a cMACS, Department of Microbial and Molecular Systems, KU Leuven, Celestijnenlaan 200F, 3001 Leuven, Belgium.

^b Department of Chemistry, KU Leuven, Celestijnenlaan 200F, 3001 Leuven, Belgium.

^c Guangzhou Institute of Energy Conversion, Chinese Academy of Sciences, No. 2, Nengyuan, Road, Tianhe District, Guangzhou 510640 P.R. China.

Simulated X-ray diffractograms

(a)



(b)

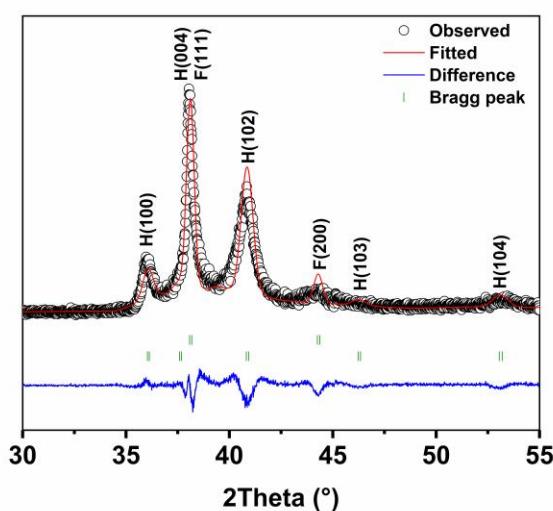


Figure S1 Simulated X-ray diffractograms based on experimental X-ray diffraction data and the space groups of fcc Ag and hcp Ag and assignment of hkl planes to the different peaks of (a) fcc Ag nanoparticles ($Fm\bar{3}m$ space group) and (b) mixed phase hcp/fcc Ag nanoparticles ($P6_3/mmc + Fm\bar{3}m$ space groups).

Capping agent

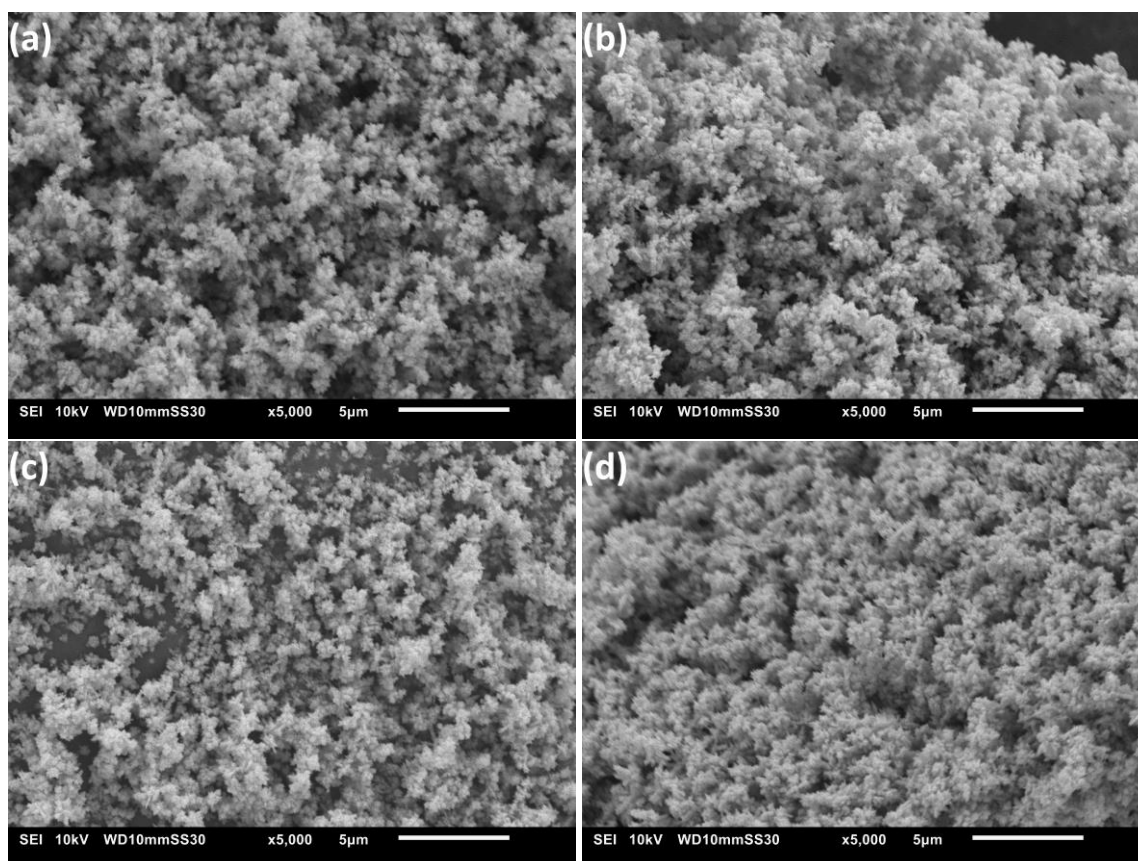


Figure S2 SEM images of Ag microparticles synthesized with different capping agents. (a) dodecanethiol, (b) oleylamine, (c) oleic acid and (d) polyvinylpyrrolidone (PVP).

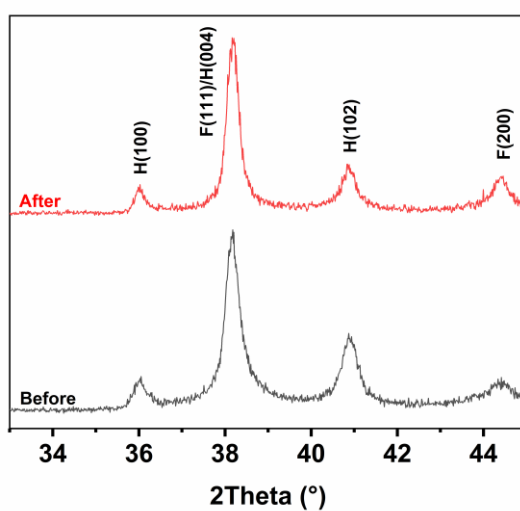


Figure S3 X-ray diffractograms showing the influence of the moment oleic acid is added to the reaction mixture. Before and after denote that oleic acid was added before or after the addition of formaldehyde and the ammonia solution and the start of the reduction of Ag^+ to metallic Ag. The X-ray diffractograms were normalized to the F(111)/H(004) peak at 38.2° .

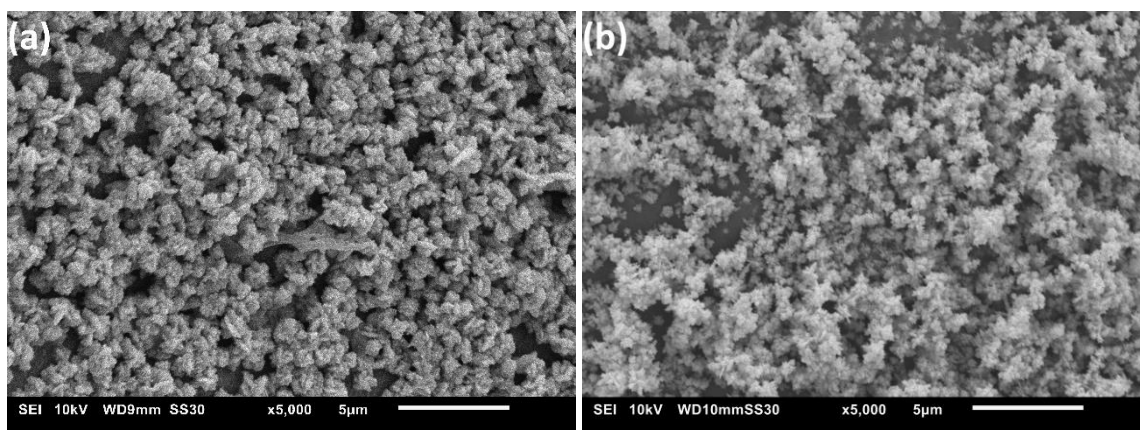


Figure S4 SEM images of oleic acid capped Ag microparticles with addition of oleic acid (a) before and (b) after the start of the reduction reaction.

pH

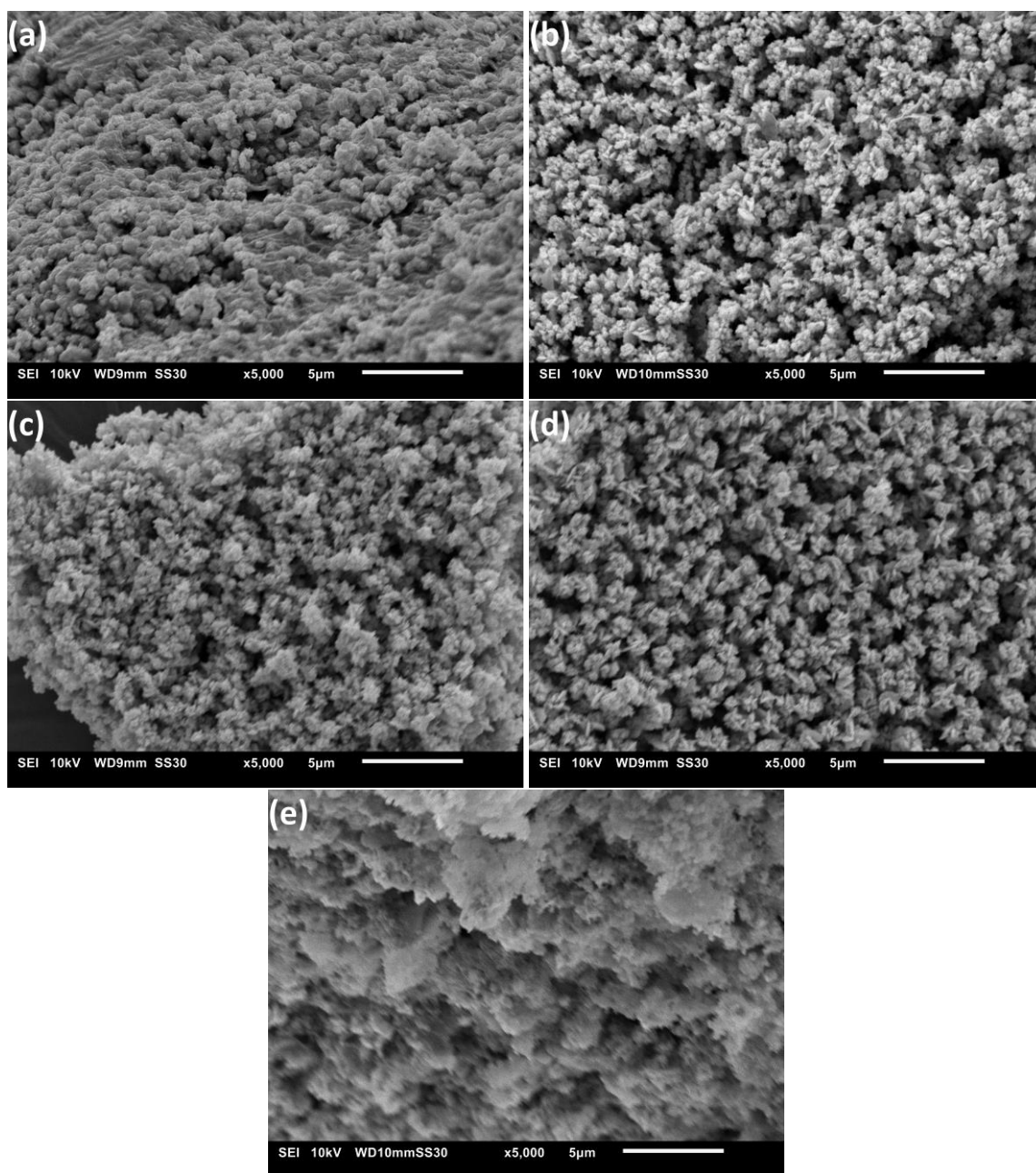


Figure S5 SEM images of oleic acid capped Ag microparticles synthesized at different pH. (a) 10.46, (b) 10.70, (c) 10.91, (d) 10.98 and (e) 11.04.

Table S1 Particle size of Ag microparticles in function of the pH. The particle size was determined by measuring 50 particles from the SEM images using ImageJ.

pH	Size (μm)
10.46	0.65 ± 0.13
10.70	0.76 ± 0.14
10.91	0.83 ± 0.12
10.98	1.01 ± 0.17
11.04	1.12 ± 0.24

Synthesis Temperature

Table S2 Fitted peak position of the F(111)/H(004) peak with fitting error for synthesis solutions with a different temperature.

Temperature (°C)	Fitted peak position (°)
25	38.134 ± 0.003
35	38.070 ± 0.006
45	38.090 ± 0.106
55	38.101 ± 0.012
65	38.109 ± 0.010
75	38.129 ± 0.013
85	38.195 ± 0.029

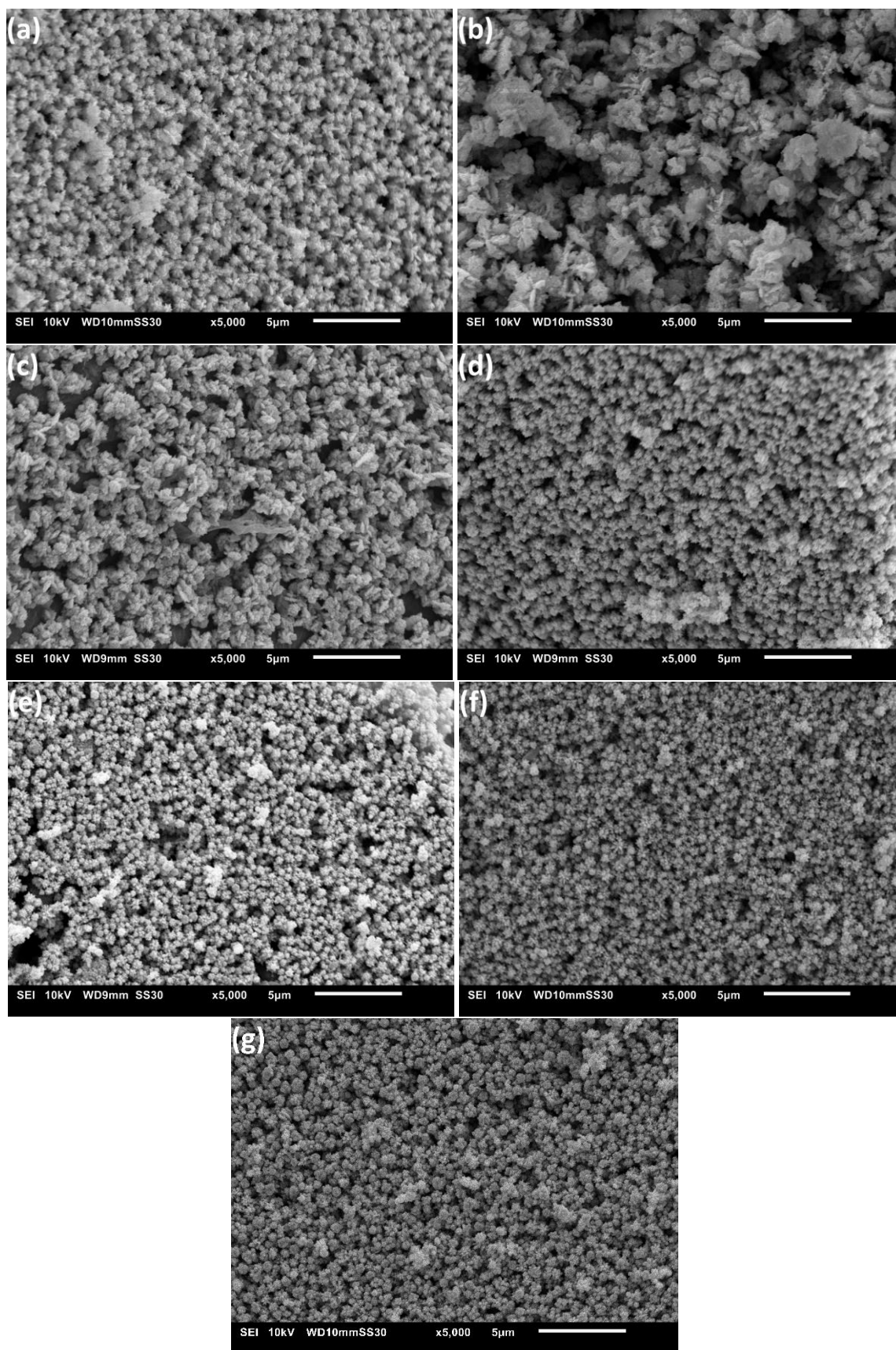


Figure S6 SEM images of oleic acid capped Ag microparticles synthesized at different synthesis temperatures. (a) 25°C, (b) 35°C, (c) 45°C, (d) 55°C, (e) 65°C, (f) 75°C and (g) 85°C.

Table S3 Particle size of Ag microparticles in function of the synthesis temperature. The particle size was determined by measuring 50 particles from the SEM images using ImageJ.

T (°C)	Size (μm)
25	0.48 ± 0.17
35	1.74 ± 0.29
45	0.79 ± 0.14
55	0.69 ± 0.10
65	0.60 ± 0.07
75	0.55 ± 0.09
85	0.53 ± 0.09

Formaldehyde to silver nitrate ratio

Table S4 Fitted peak position of the F(111)/H(004) peak with fitting error for synthesis solutions with a different formaldehyde to silver nitrate ratio.

n(Fa/AgNO ₃)	Fitted peak position (°)
46	38.079 ± 0.002
68	38.062 ± 0.002
91	38.082 ± 0.003
137	38.082 ± 0.005
183	38.130 ± 0.042
228	38.140 ± 0.103

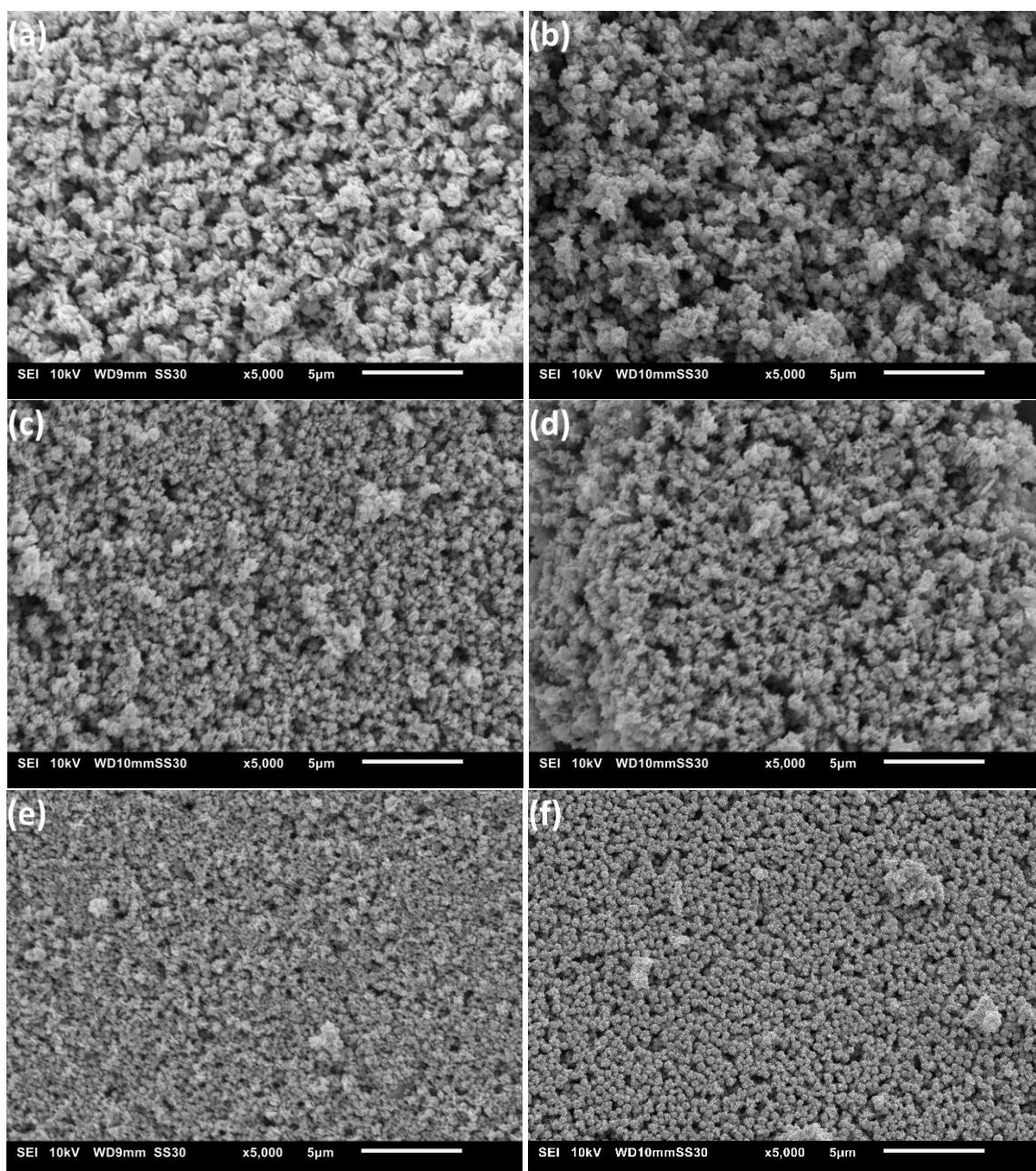


Figure S7 SEM images of oleic acid capped Ag microparticles synthesized at different molar reductant-to-precursor ratios. (a) 46, (b) 68, (c) 91, (d) 137, (e) 183 and (f) 228.

Table S5 Particle size of Ag microparticles in function of the formaldehyde to silver nitrate ratio. The particle size was determined by measuring 50 particles from the SEM images using ImageJ.

n(Fa/AgNO ₃)	Size (μm)
46	1.23 ± 0.20
68	0.89 ± 0.16
91	0.58 ± 0.10
137	0.61 ± 0.11
183	0.45 ± 0.12
228	0.38 ± 0.05

Particle size distribution of the optimized hcp Ag microparticles

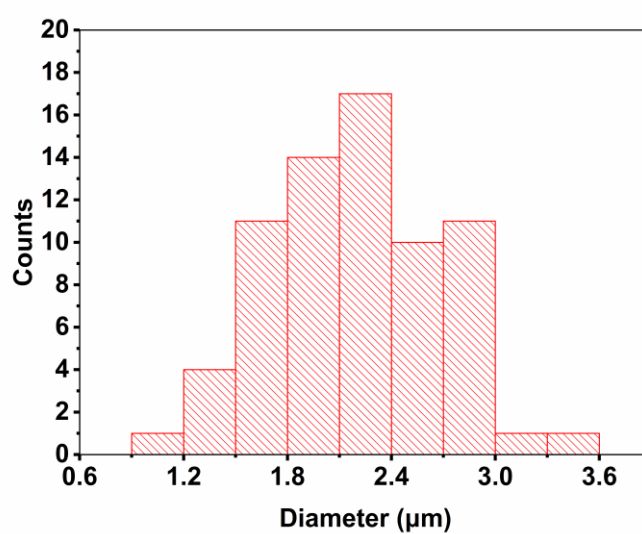


Figure S8 Histogram showing the particle size distribution. The particle size was determined by measuring 70 particles from the SEM images using ImageJ.

TEM and SAED of the optimized hcp Ag microparticles

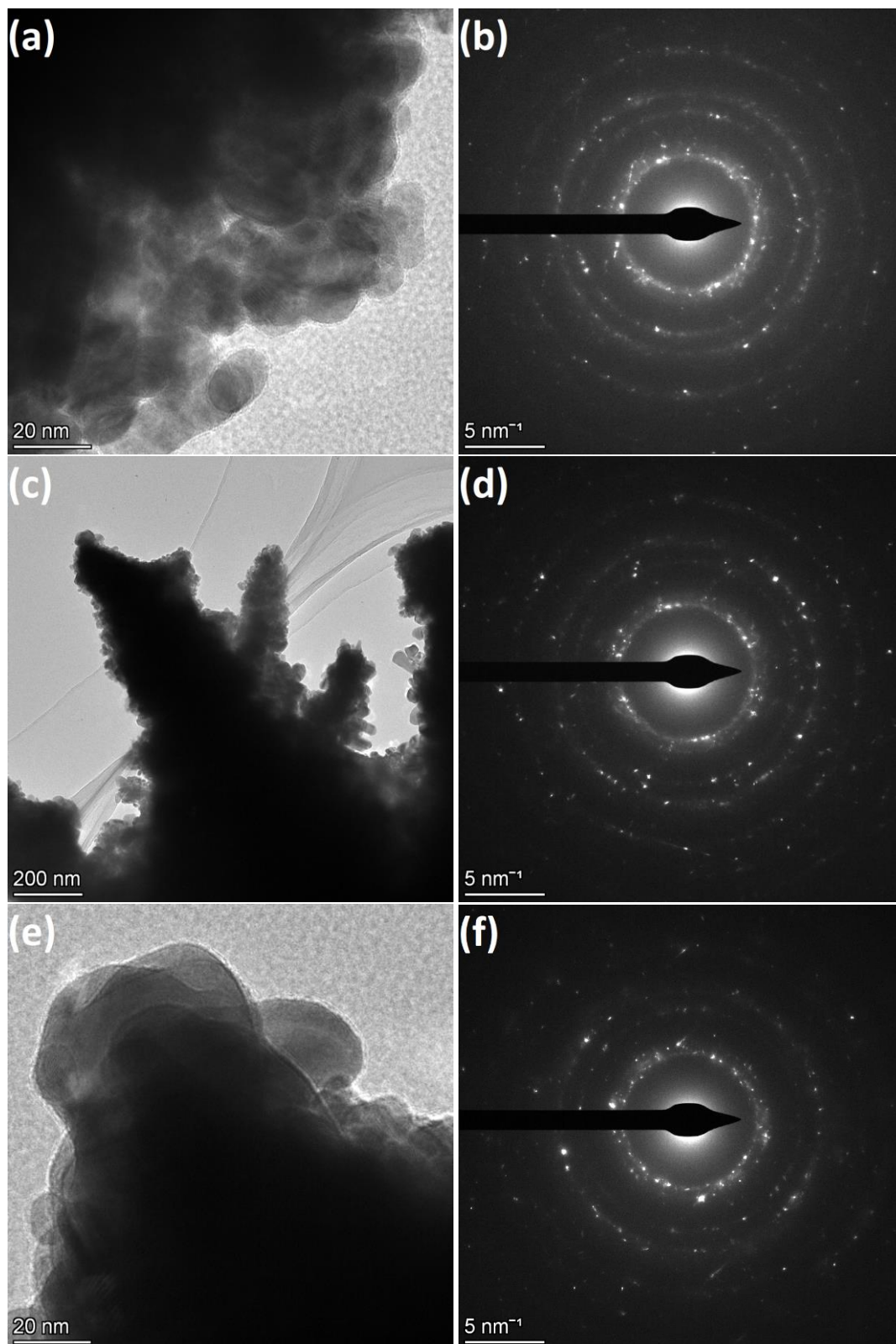


Figure S9 TEM images of hcp Ag microparticles (a) near the core (position 1), (c) in the middle of a tip (position 2) and (e) at the end of a tip (position 3). SAED images of hcp Ag microparticles at (b) position 1 (TEM image a), (d) position 2 (TEM image c) and (f) position 3 (TEM image e).

Table S6 Measured d-spacing from the SAED data, assigned miller indices and calculated d-spacing of the corresponding crystal planes based on the XRD data. Rings with a bigger diameter as ring 3 all correlated with reflections with 2Theta bigger than 70° and were omitted for simplicity since they were not measured with XRD.

Position	No.	d-spacing (measured) (Å)	Miller-indices(hkl)	d-spacing (calculated) (Å)
1	1	2.38	H(004)/F(111)	2.39/2.36
	2	1.96	F(200)	2.05
	3	1.42	F(220)	1.44
2	1	2.37	H(004)/F(111)	2.39/2.36
	2	2.03	F(200)	2.05
	3	1.42	F(220)	1.44
3	1	2.37	H(004)/F(111)	2.39/2.36
	2	2.04	F(200)	2.05
	3	1.43	F(220)	1.44

Stability of the hcp Ag microparticles under ambient conditions

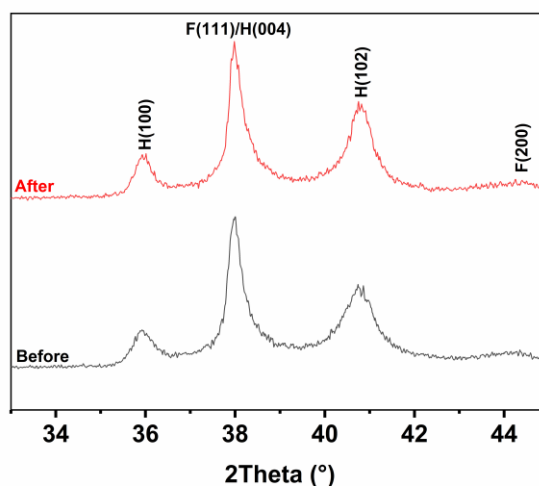


Figure S10 X-ray diffractograms of the hcp Ag microparticles before and after storage under ambient conditions for 20 months. The X-ray diffractograms were normalized to the F(111)/H(004) peak at 38.2°.

Table S7 Amount of hcp Ag calculated via fitting of the H(102) peak and peak position of the F(111)/H(004) peak with fitting error of the as synthesized hcp microparticles before and after storage for 20 months under ambient conditions.

	$A_{\text{hcp}}/A_{\text{main}}$	Fitted peak position F(111)/H(004) (°)
Before	0.712	37.997 ± 0.002
After	0.712	38.004 ± 0.007

Stability of the hcp Ag microparticles in various solvents

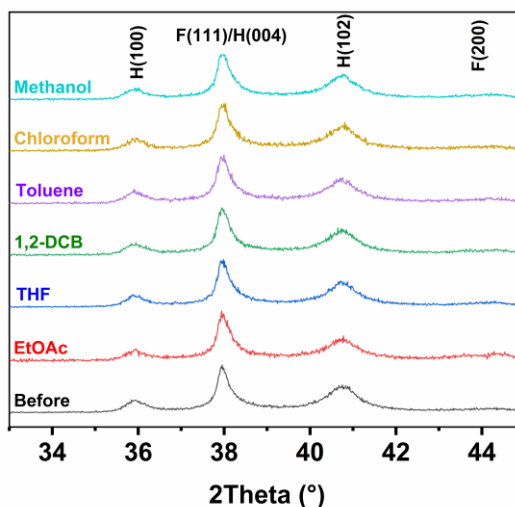


Figure S11 X-ray diffractograms showing the stability of the hcp Ag microparticles in various solvents. The tested solvents are ethyl acetate (EtOAc), tetrahydrofuran (THF), 1,2-dichlorobenzene (1,2-DCB), toluene, chloroform and methanol. The X-ray diffractograms were normalized to the F(111)/H(004) peak at 38.2°.

Table S8 Amount of hcp Ag calculated via fitting of the H(102) peak and peak position of the F(111)/H(004) peak with fitting error of the as synthesized hcp microparticles before and after stability tests in various solvents.

	$A_{\text{hcp}}/A_{\text{main}}$	Fitted peak position(111)/H(004) (°)
Before	0.712	37.997 ± 0.002
Ethyl acetate	0.710	38.005 ± 0.005
Tetrahydrofuran	0.710	38.004 ± 0.006
1,2-Dichlorobenzene	0.711	37.998 ± 0.006
Toluene	0.709	37.998 ± 0.007
Chloroform	0.711	38.007 ± 0.006
Methanol	0.711	38.006 ± 0.006

Stability of the hcp Ag microparticles under increased pressures

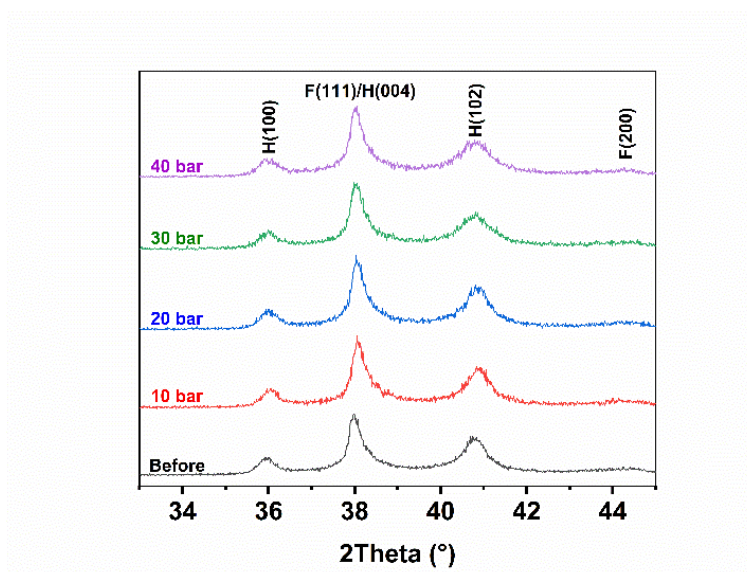


Figure S12 X-ray diffractograms showing the stability of the hcp Ag microparticles under various pressures of N₂ gas. The X-ray diffractograms were normalized to the F(111)/H(004) peak at 38.2°.

Table S9 Amount of hcp Ag calculated via fitting of the H(102) peak and peak position of the F(111)/H(004) peak with fitting error of the as synthesized hcp microparticles before and after stability tests under increased N₂ pressure.

	$A_{\text{hcp}}/A_{\text{main}}$	Fitted peak position(111)/H(004) (°)
Before	0.712	37.997 ± 0.002
10 bar	0.712	38.006 ± 0.007
20 bar	0.712	38.003 ± 0.007
30 bar	0.712	38.001 ± 0.007
40 bar	0.711	38.009 ± 0.006

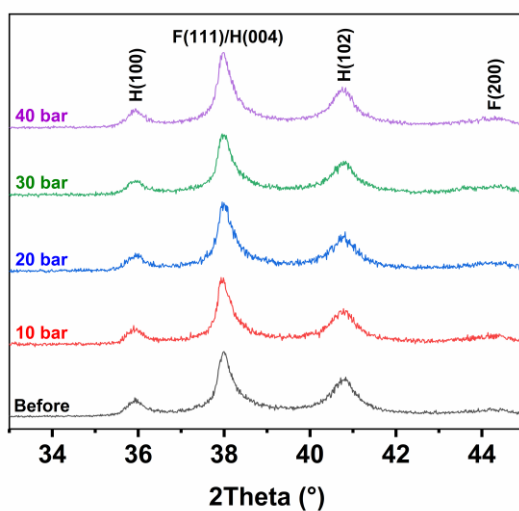


Figure S13 X-ray diffractograms showing the stability of the hcp Ag nanoparticles under various pressures of H₂ gas. The X-ray diffractograms were normalized to the F(111)/H(004) peak at 38.2°.

Table S10 Amount of hcp Ag calculated via fitting of the H(102) peak and peak position of the F(111)/H(004) peak with fitting error of the as synthesized hcp nanoparticles before and after stability tests under increased H₂ pressure.

	$A_{\text{hcp}}/A_{\text{main}}$	Fitted peak position(111)/H(004) (°)
Before	0.712	37.997 ± 0.002
10 bar	0.710	38.009 ± 0.006
20 bar	0.709	38.003 ± 0.007
30 bar	0.712	38.005 ± 0.006
40 bar	0.711	38.004 ± 0.006

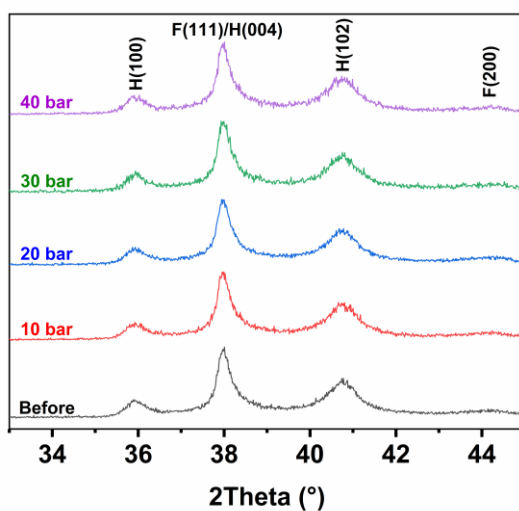


Figure S14 X-ray diffractograms showing the stability of the hcp Ag microparticles under various pressures of O₂ gas. The X-ray diffractograms were normalized to the F(111)/H(004) peak at 38.2°.

Table S11 Amount of hcp Ag calculated via fitting of the H(102) peak and peak position of the F(111)/H(004) peak with fitting error of the as synthesized hcp microparticles before and after stability tests under increased O₂ pressure.

	$A_{\text{hcp}}/A_{\text{main}}$	Fitted peak position(111)/H(004) (°)
Before	0.712	37.997 ± 0.002
10 bar	0.709	38.012 ± 0.007
20 bar	0.710	38.013 ± 0.006
30 bar	0.711	38.023 ± 0.007
40 bar	0.711	38.022 ± 0.007

Thermal stability of the hcp Ag microparticles

The thermal stability of the hcp Ag microparticles was tested at the following temperatures: 30°C, 50°C, 60°C, 70°C, 80°C, 90°C, 95°C, 100°C, 105°C, 110°C, 115°C, 120°C, 125°C, 130°C, 135°C, 140°C, 145°C, 150°C, 160°C, 170°C, 180°C, 190°C, 200°C, 210°C, 220°C, 230°C. Only X-ray diffractograms in increments of 20°C were shown in the paper for simplicity, the X-ray diffractograms not shown there can be seen in Figure S14.

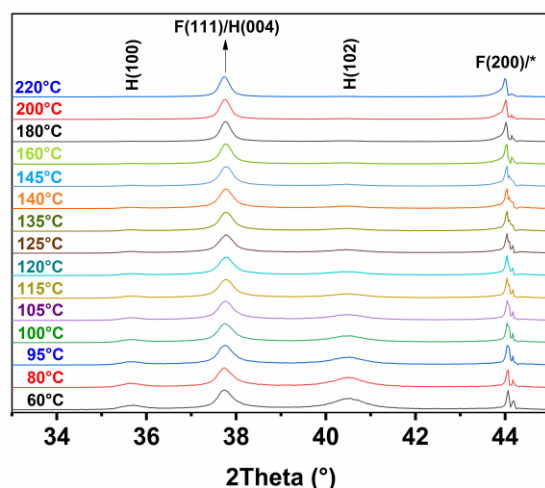


Figure S15 In-situ X-ray diffractograms of oleic acid capped hcp Ag microparticles at various temperatures under nitrogen atmosphere. * denotes a peak attributed to the sample holder.

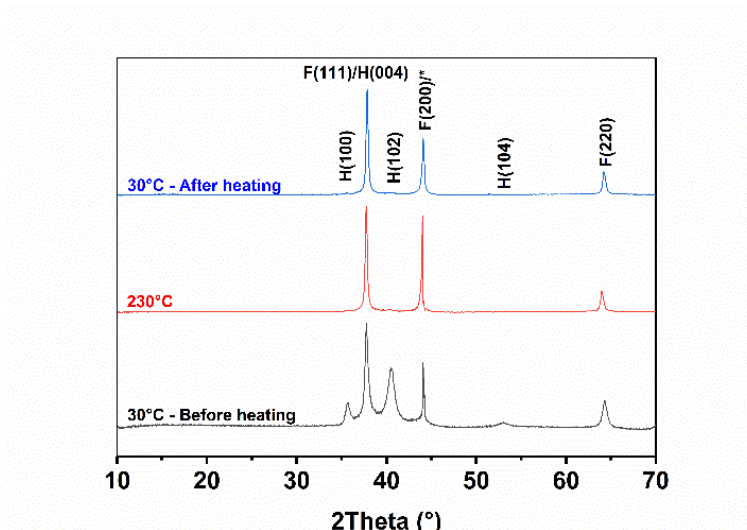


Figure S16 Comparison of the X-ray diffractograms of hcp Ag microparticles at 30°C before heating, at 230°C and at 30°C after heating to 230°C. * denotes a peak attributed to the sample holder. The X-ray diffractograms were normalized to the F(111)/H(004) peak at 38.2°.

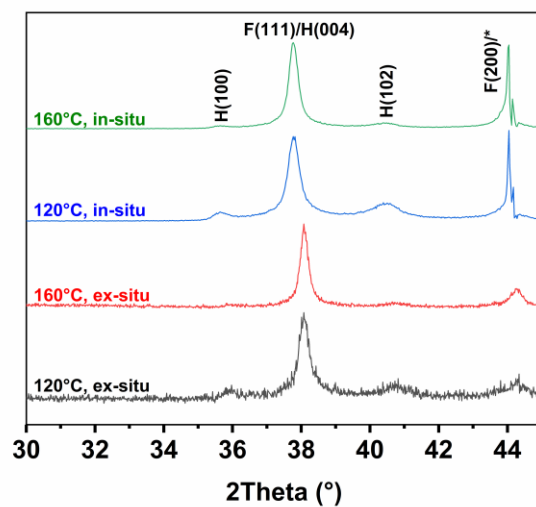


Figure S17 Comparison of the X-ray diffractograms of hcp Ag microparticles at 120°C and 160°C via in-situ and ex-situ XRD measurements. * denotes a peak attributed to the sample holder. The X-ray diffractograms were normalized to the F(111)/H(004) peak at 38.2°.

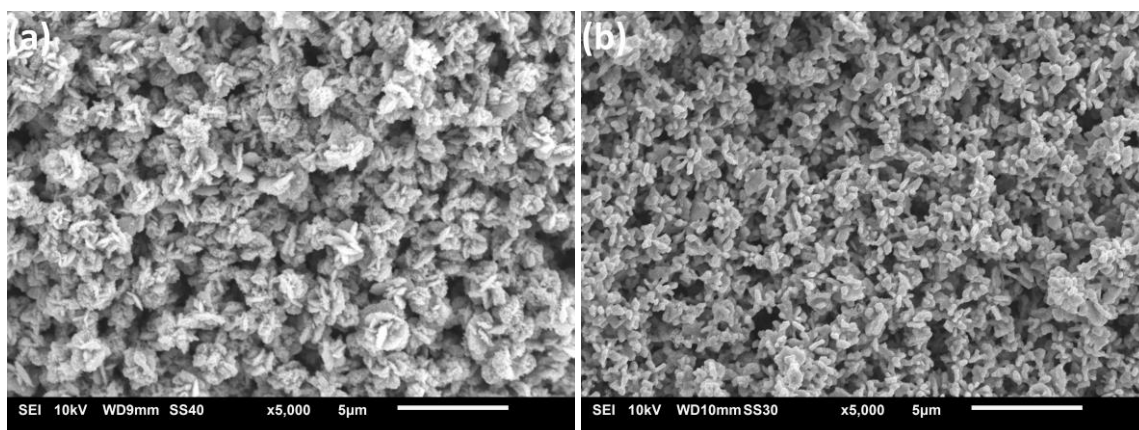


Figure S18 SEM images of the fully optimized hcp Ag microparticles (a) before and (b) after thermal phase transition under nitrogen atmosphere.